Stress transfer in the western boundary of Bayan Har Block in Tibet Plateau from the 2008 to 2020 Yutian Earthquake sequence in China

Ke Jia[1*], Shiyong Zhou[2], Jiancang Zhuang[3], Changsheng Jiang[4]

1 School of Automation, Northwestern Polytechnical University, Xi'an 710129, China

2 School of Earth and Space Sciences, Peking University, Beijing 100871, China

3 The Institute of Statistical Mathematics, 10-3 Midori-Cho, Tachikawa, Tokyo 190-8562, Japan

4 Institute of Geophysics, China Earthquake Administration, No.5 Minzu Daxue Nan Road, Haidian District, Beijing 100086, China

*Corresponding author: jk@nwpu.edu.cn

Key points:

1. Four M>=6.0 occurred in an intersection of multiple groups of large strike-slip active faults with different strikes from 2008 to 2020.
2. Stress interactions between those four earthquakes are investigated.
3. The statistical insight provides a good cross reference for triggering mechanism due to its objectivity and small uncertainties.

Abstract

Eight M≥7.0 earthquakes have occurred around Bayan Har block since 2000, resulting huge casualties and countless economic loss. Specifically, four M≥6.0 earthquakes occurred near the western boundary of Bayan Har block from 2008 to 2020. Stress interactions among them are comprehensively investigated by applying ETAS (epidemic-type aftershock sequence) model and calculating dCFS (Coulomb failure stress change). The viscoelastic dCFS induced by proceeding Yutian earthquakes on hypocenters of 2012, 2014 and 2020 Yutian earthquakes are -1.5004×10^{-4}, 3.5820×10^{-3} and 1.4770×10^{-1} MPa, respectively. The background probabilities of 2008, 2012, 2014 and 2020 Yutian earthquakes are 0.87, 0.97, 1.5×10^{-3} and 8.7×10^{-5}, respectively. Combining those two kinds of evidence, we conclude that 2008 and 2012 Yutian earthquakes are more like background earthquakes and 2014 and 2020 Yutian earthquakes are triggered by proceeding Yutian earthquakes.

Plain Language Summary

Along the boundaries of Bayan Har block, there have be eight big earthquakes since 2000, resulting huge casualties and countless economic loss. At its western boundary, four earthquakes with magnitude larger than 6.0 occurred since 2008 in a small but complex region (Yutian region). A large earthquake could be triggered by other strong earthquakes or occurred due to tectonic loading. Whether those four large earthquakes were triggered is an important question to assess regional seismic hazard. We use two kinds of methods to address this issue. One is direct calculation of stress transfer among those earthquakes and another one is estimation of probabilities being a background event (an event is driven by tectonic loading) using statistically analysis from observed earthquake catalog. We find that the stress transfer from proceeding major earthquakes to 2012 Yutian earthquake is small, while that to 2014 and 2020 Yutian earthquake are moderate. The background probabilities of 2008 and 2012 Yutian earthquakes are high, while background probabilities of 2014 and 2020 Yutian earthquakes are very low. Thus, we conclude that 2008 and 2012 Yutian earthquakes are more like background earthquakes and 2014 and 2020 Yutian earthquakes are triggered by

proceeding Yutian earthquakes.

1. Introduction

Stress interaction among major earthquakes have been paid more and more attentions. A lot of case studies (e.g., the 1992 Landers and 1999 Hector Mine earthquake in the US (*Freed and Lin*, 2001); the 2008 Wenchuan, 2013 Lushan and 2017 Jiuzhaigou earthquake in China (*Jia et al.*, 2014; *Jia et al.*, 2018; *Wan and Shen*, 2010; *Wang et al.*, 2014b); the 2010-2011 Canterbury Earthquake Sequence in New Zealand (*Quigley et al.*, 2016); the foreshock and mainshock of the 2019 Ridgecrest earthquake in the US (*Pope and Mooney*, 2020; *Ramos et al.*, 2020)) have been investigated under the framework of Coulomb failure hypothesis, which assumes positive dCFS promotes occurrence of earthquake and negative dCFS delays that. Meanwhile, many researchers have shown that the calculated dCFSs are positively correlated with observed seismicity rate changes (*Harris*, 1998; *Jia et al.*, 2014; *Kroll et al.*, 2017; *Pollitz and Cattania*, 2017; *Stein*, 1999; *Toda et al.*, 2012; *Toda et al.*, 2005; *Zhuang et al.*, 2005). That means observed seismicity increases in regions with positive dCFSs and decreases in regions with negative dCFSs. In this way, calculations of dCFS and seismicity rate changes could help to clarify stress interactions between earthquakes and faults, and further to evaluate seismic hazard.

The recent June 26, 2020 Mw 6.3 Yutian earthquake (hereafter 20YT) occurred in western Kunlun mountains, NW Tibet, China. Three other M≥6.0 earthquakes occurred near the epicenter of the 20YT since 2008. The March 20, 2008 Mw 7.1 Yutian earthquake (hereafter 08YT), one of the largest normal earthquakes on the continents, occurred 94 km away to the west from the epicenter of 20YT. The August 12, 2012 Mw 6.2 Yutian earthquake (hereafter 12YT) and the February 12, 2014 Mw 6.9 Yutian earthquake (hereafter 14YT) occurred 25 km and 61 km away to the north from the epicenter of 20YT (Figure 1). The source region of those four earthquakes at the western boundary of the Bayan Har block experiences an extensive stress field bounded by two strike-slip fault system: the Altyn Tagh fault in the north and the Longmu-Gozha Co fault in the south (*Taylor and Yin*, 2009), which further

84 relates to collision of India plate and Eurasia plate. This area is the intersection of multiple
85 groups of large strike-slip active fault belts with different strikes. The 08YT, 12 YT, 14 YT
86 and 20YT sequence provides an opportunity to case study of the Coulomb failure hypothesis
87 and help to evaluate the seismic hazard of Bayan Har block.
88

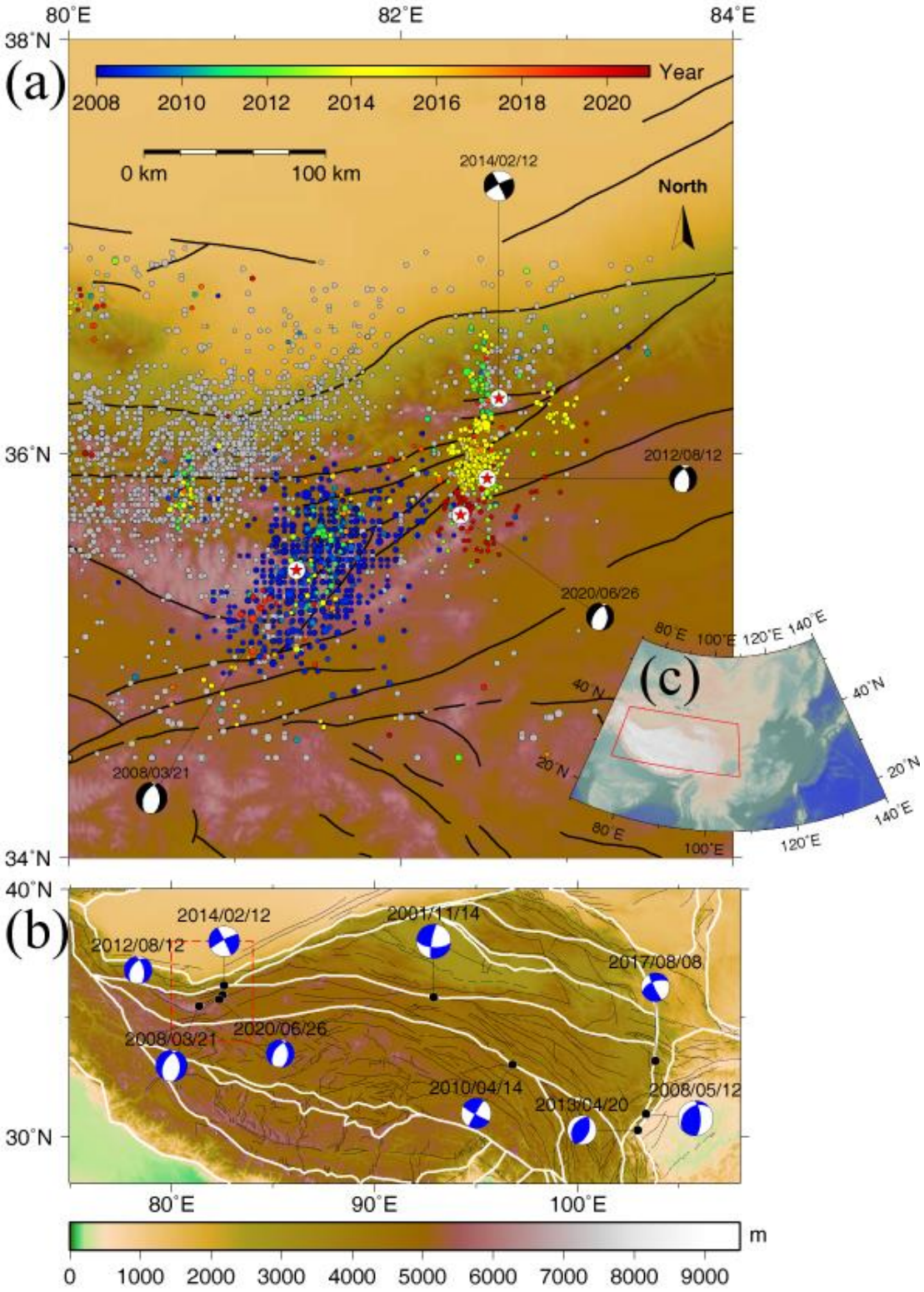

Figure 1 Tectonic settings of the Yutian region and Bayan Har block. (a) The gray filled circles represent earthquakes with M≥3.5 from 1 January 1970 to 31 December 2007. The color filled circles are earthquakes with M≥3.5 from 1 January 2008 to 23 August 2020, and colors represent their occurrence time. The four red stars represent the epicenters of the 2008,

2012, 2014 and 2020 Yutian earthquakes, and their focal mechanisms are from Global Centroid Moment Tensor. The black lines represent major faults (*Zhang et al.*, 2003). (b) Nine major earthquakes (M⩾7.0 except for the Yutian region) occurred at boundaries of the Bayan Har block since 2000. The red dashed polygon represents region of (a). (c) Red solid polygon represents region of (b) with respect to mainland China.

Previous studies have shown stress triggering between 08YT and 14YT (*Li et al.*, 2015; *Wang et al.*, 2017; *Zhao et al.*, 2016) and seismicity rate change following 08YT, 12YT and 14YT (*Jiang et al.*, 2014; *Zhao et al.*, 2016). Using a three-dimensional viscoelastic finite element model, *Li et al.* (2015) showed that dCFS induced by 08YT on slip direction of the 14YT exceeded 0.01 MPa (the earthquake triggering threshold). They implied an apparent triggering effect of 08YT to 14YT and suggested the 14YT was advanced 21.4-24.9 years by the 08YT (*Li et al.*, 2015). *Zhao et al.* (2016) claimed that the 14YT located at triggering zone caused by the 08YT and observed spatial distributions of aftershocks of those two major events were well correlated with positive dCFS. *Wang et al.* (2017) examined coseismic, postseismic and interseismic dCFSs induced by 08 YT on the 14 YT and implied a triggering relationship between them.

However, roles of the 12YT and 20YT in stress interaction with other Yutian earthquakes have not been investigated. More importantly, whether the occurrence of the 20YT is triggered by proceeding Yutian earthquakes or a background event may lead different evaluation of regional seismic hazard. If the 20YT is a triggered event, the local stress level may be still in a condition of post-seismic releasing or adjustment. On the other hand, an independent 20YT implies a continuous tectonic loading and releasing. Especially for a relatively small region, occurrences of four M≥6.0 earthquakes within 13 years are rare and provide an opportunity to study stress interactions (both static and viscoelastic stress changes) among them. Furthermore, together with seismicity analysis, those two kinds of evidence could be useful to understand occurrence of the 20YT and seismic hazard of Bayan Har block.

Here in this manuscript, the seismicity rate changes in Yutian region from 2008 to 2020, the

dCFS at hypocenter of the 20YT induced by the proceeding Yutian earthquakes (08YT, 12YT and 14YT), and the correlations between them are comprehensively investigated. The ETAS model and stochastic declustering method are used to obtain the background seismicity rate change. The co-seismic (elastic) and post-seismic (viscoelastic) dCFS are calculated in an elastic/viscoelastic layered half-space. Uncertainties of dCFS are investigated by considering different friction coefficients. Based on the results of dCFS and seismicity analysis, we discuss several key points and draw our conclusion.

2. Detection of seismicity rate changes by using the ETAS model

2.1 Space-time ETAS model

The space-time ETAS model, proposed by *Ogata* (1998), combines several classic statistical laws in seismicity, including the Omori-Utsu law, productivity law and Gutenberg-Richter law. The ETAS model assumes each earthquake could trigger its own aftershocks with an ability corresponding to its magnitude. The ETAS model has been successfully applied in many regions and become a standard model to analyze spatial and temporal seismicity (*Jia et al.*, 2014; *Jia et al.*, 2018; *Ogata*, 2004; *Ogata and Zhuang*, 2006; *Zhuang et al.*, 2005; *Zhuang et al.*, 2004). Details of the space-time ETAS model could be referred to *Ogata and Zhuang* (2006).

After obtaining final estimations of parameters of the ETAS model, the background probability (an event is regarded as a background event with a probability) of the jth event φ_j, can be estimated by

$$\varphi_j = \frac{\mu\left(x_j, y_j\right)}{\lambda\left(t_j, x_j, y_j\right)}, \tag{1}$$

where $\mu\left(x_j, y_j\right)$ is the background and total seismicity rate at the location of *j*th event and $\lambda\left(t_j, x_j, y_j\right)$ is the total seismicity rate at the location and occurrence time of *j*th event.

2.2 Fitting ETAS model

A polygon region (80.0°-83.5°E, 34.5°-37.0°N) is selected to present the Yutian region for

model fitting and seismicity analysis. The selected region should contain enough number of events for model fitting, and avoids influence from other large earthquakes or faults at the same time. The time range is from 1 January 1980 to 23 August 2020 covering occurrences of all the four M≥6.0 earthquakes (Figure S1). The cut-off magnitude of seismic catalog is carefully selected because using an incomplete catalog may lead instable estimation of model parameters (*Ogata*, 1998; *Utsu et al.*, 1995). *Harte* (2015) and *Sornette and Werner* (2005) also declaimed that parameter estimation may contain bias by using a larger cut-off magnitude than the triggering boundary magnitude. Thus, we choose the complete magnitude as the cut-off magnitude to minimize abovementioned problems. The maximum curvature technique (*Wiemer*, 2001; *Wiemer and Wyss*, 2000) is applied in the Yutian region to estimate the temporal complete magnitude (Figure S2). From Figure S2, the complete magnitude is above 3.5 from 1980 to 2020, and the we choose the complete magnitude with 3.5.

The catalog used in this study is downloaded from China Earthquake Data Center (CEDC, http://data.earthquake.cn/index.html), and events above complete magnitude are selected within spatiotemporal range to fit the ETAS model by maximum likelihood method. The final estimations of model parameters for Yutian region are $\hat{A}=0.466$ (events), $\hat{c}=0.045$ (day), $\hat{\alpha}=1.075$ (m^{-1}), $p=1.143$, $\hat{D}=2.181\times10^{-2}$ (deg^2), $\hat{q}=2.537$, and $\hat{\gamma}=0.116$ (m^{-1}).

2.3 Background seismicity rate in the Yutian region

Background probabilities of earthquakes with Mw≥6.0 are listed in Table S1 and spatiotemporal distributions of background probabilities are shown in Figure S3. From Figure S3, a lot of aftershocks have been effectively distinguished. The background probabilities of 08YT, 12YT, 14YT and 20YT are 0.87, 0.97, 1.5×10^{-3} and 8.7×10^{-5}, respectively. This implies that the 08YT and 12YT are more like background earthquakes and 14YT and 20YT are triggered events in a view of ETAS model.

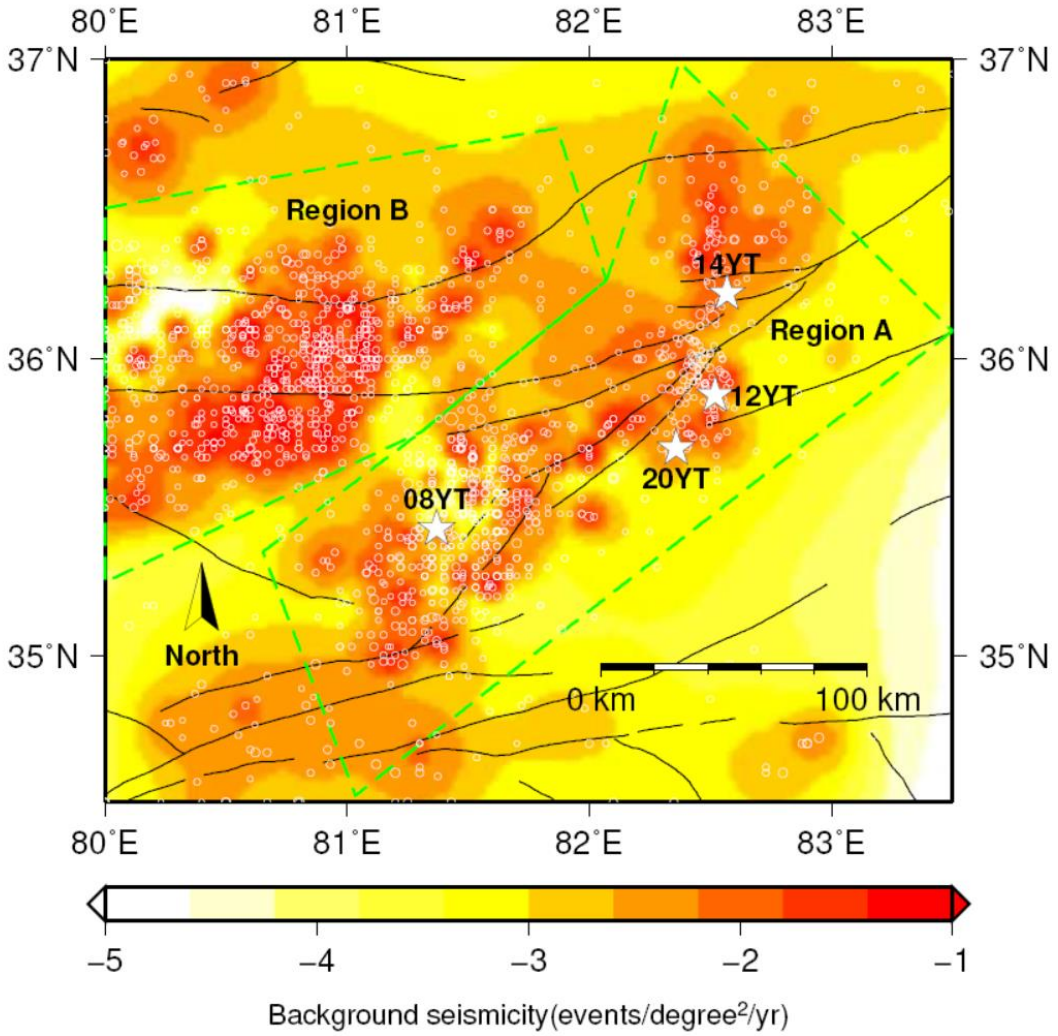

Figure 2 Estimated spatial background seismicity in Yutian region. White circles represent earthquake with magnitude larger than 3.5 from 1970 to 2020. Four white stars indicate 08YT, 12YT, 14YT and 20YT. Black lines are active faults. Region A and B are marked with green dashed lines for seismicity analysis. Note that the background seismicity rate is represented by the logarithm scale.

The spatial background seismicity is shown in Figure 2. The epicenters of 08YT, 12YT, 14YT and 20YT suffer highest background seismicity (approximately 0.1 $M \geq 3.5$ events/degree^2/yr), where the fault traces are also dense. The spatial background seismicity in Yutian region shows a relatively high level resulting from the complex stepover zone with multiple normal faults (*Bie and Ryder*, 2014; *Tapponnier et al.*, 2001; *Xu et al.*, 2013).

The cumulative background probabilities of earthquakes $S(t)$, proposed by *Zhuang et al.* (2005), is written as

$$S(t) = \sum_{t_j < t} \varphi_j \tag{2}$$

We assume that the background seismicity rate is time-invariant in a stable region, thus $S(t)$ constantly increases with time. Changes in slope of $S(t)$ curve imply changes in background seismicity rate: an increased slope represents an activation of the background seismicity and a decreased slope means background quiescence.

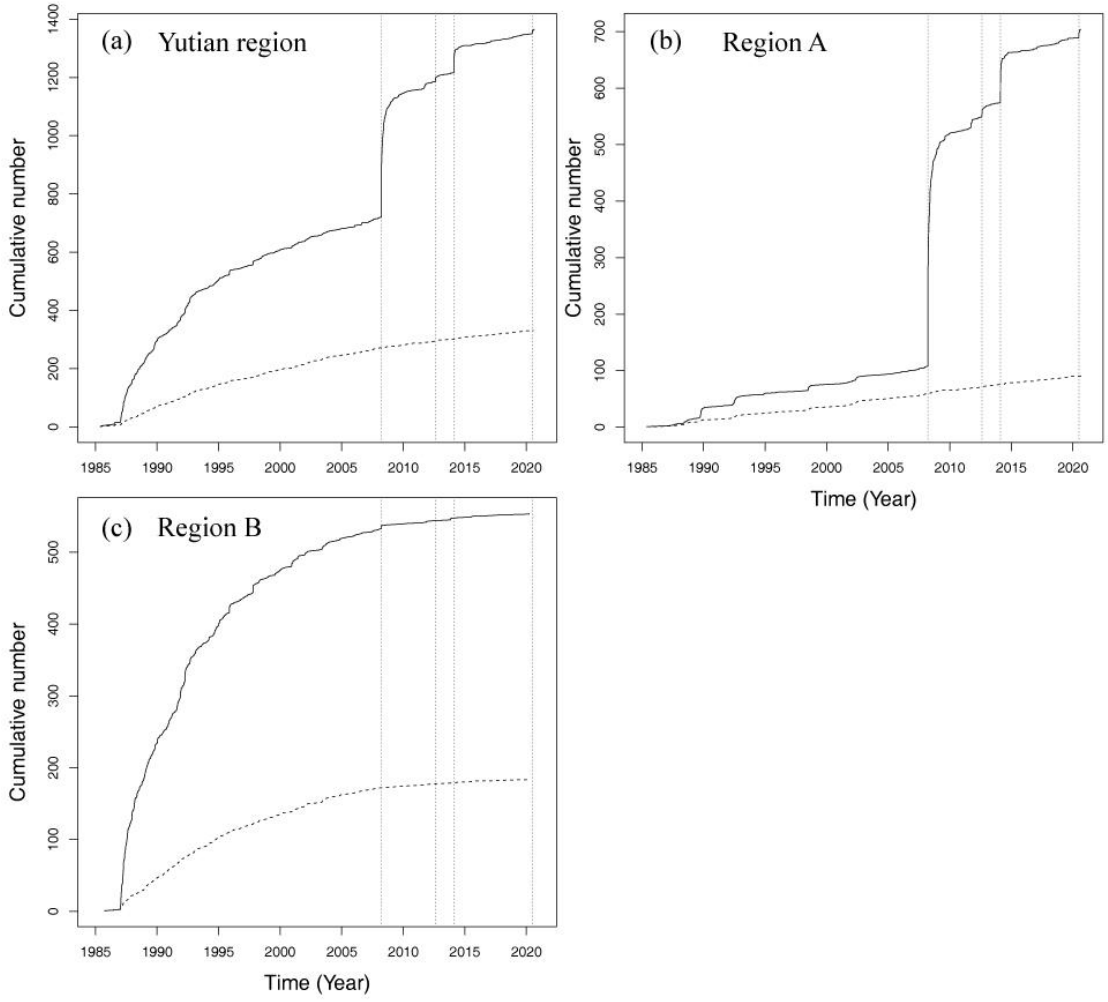

Figure 3 Cumulative number of earthquakes and background probabilities for the Yutian region (a), region A (b) and region B (c) marked in Figure 2. The black line represents cumulative number of all earthquakes in the study region from 1985 to 2020 and the dashed

line represents cumulative number of background probabilities. The four vertical dashed lines indicate occurrence time of the 08YT, 12YT, 14YT and 20YT from left to right.

Figure 3 shows cumulative number of earthquakes and background probabilities in the Yutian region and two sub-regions marked in Figure 2. From Figure 3(a), it could be seen that the cumulative number of earthquakes in Yutian region dramatically increases after each major earthquake, while the rate of background probability keeps stable from 1990 to 2020 and is not affected by the major earthquakes. This finding suggests that the Yutian region experiences a constant background seismicity under a stable tectonic environment. The relationship between those four major Yutian earthquakes will be discussed later along with the calculations of dCFS. Region A indicates the fault zone of those four Yutian earthquakes, experiencing a constant background seismicity rate (Figure 3(b)). Region B shows a decrease of background seismicity after the 08YT, which might be caused by a negative dCFS induced by 08YT (Figure 4(a) and (b)).

3. Coulomb Failure Stress change

To further investigate stress interaction among the 2008, 2012, 2014 and 2020 Yutian earthquake, we calculate the static (coseismic) and viscoelastic (postseismic) Coulomb stress changes induced by proceeding events. The lower crust and upper mantle are considered to be layered and viscoelastic. The proposed viscoelastic model contains an elastic upper crust, a viscoelastic lower crust with viscosity to be $1\times10^{18}Pa\cdot s$ and a viscoelastic upper mantle with a viscosity value of $1\times10^{20}Pa\cdot s$, respectively (*Jia et al.*, 2012; *Xiong et al.*, 2010).

3.1 Method of calculation of dCFS

Given the shear stress change $d\tau_{shear}$ (positive in the sense of motion of the relevant fault) and the normal stress change $d\tau_{normal}$ (positive for extension), the dCFS can be calculated by (*Harris*, 1998; *Steacy et al.*, 2005),

$$dCFS = d\tau_{shear} + \mu\left(d\tau_{normal} - (\beta/3)\sum d\tau_{ii}\right) \quad (3)$$

where μ is the friction coefficient and β is Skempton's coefficient. If the medium is homogeneous and the fault zone materials are ductile, as discussed in *Harris* (1998) (formula (3), (4) and (5) therein), the dCFS could be simply calculated using,

$$dCFS = d\tau_{shear} + \mu' d\tau_{normal} \quad (4)$$

where μ' is the apparent coefficient of friction and $\mu' = \mu(1-\beta)$.

It is noteworthy that the static and viscoelastic stress changes induced by the 2008/2012/2014 Yutian earthquakes are mainly considered in this manuscript. Other possible mechanisms (e.g., dynamic stress changes, stress changes driven by afterslips or fluid emigration), which also may contribute to seismicity rate changes, have not been considered.

3.2 Stress interaction among four Yutian earthquakes

We have comprehensively investigated stress transfer among the 08YT, 12YT, 14YT and 20YT. That means both static and viscoelastic dCFSs induced by proceeding Yutian earthquakes are calculated at hypocenters of later Yutian earthquakes (Table 1). The finite fault source model of the 2008 Yutian earthquake, provided by *Elliott et al.* (2010), is jointly inverted by the InSAR and body wave data. The finite fault source model of the 2014 Yutian earthquake is estimated by inverting teleseismic data (*Zhang et al.*, 2014). The synthetic slip model 2012 Yutian earthquake is estimated based on the empirical relations of *Wells and Coppersmith* (1994), because of lack of published finite fault model. The resolving depths of 12YT, 14YT and 20YT are 15 km, 20km and 15km, respectively. The project planes are selected from focal mechanisms of GCMT. The friction coefficient is set to be 0.4 and Skempton's coefficient is set to be 0.5. We have also tested different values of friction coefficient in Supplementary Information (Table S2-S3, Figure S4-S6) and discussed uncertainties in Discussion section.

Table 1 dCFS of four major Yutian earthquakes (MPa)

260

	08YT		12YT		14YT		Proceeding Yutian earthquake
	static	viscoelastic	static	viscoelastic	static	viscoelastic	Combined*
12YT	1.0267 ×10^{-3}	-1.5004× 10^{-4}	\	\	\	\	-1.5004×10^{-4}
14YT	-7.4685 ×10^{-3}	2.6181× 10^{-3}	3.1498 ×10^{-4}	9.6390× 10^{-4}	\	\	3.5820×10^{-3}
20YT	2.9825 ×10^{-3}	7.3391× 10^{-3}	3.4833 ×10^{-2}	3.5089× 10^{-2}	1.0658 ×10^{-1}	1.0523× 10^{-1}	1.4770×10^{-1}

261 *"Combined" means viscoelastic dCFS induced by three proceeding Yutian earthquakes.

262

263 From Table 1, at the hypocenter of the 12YT, the static and viscoelastic dCFSs induced by
264 08YT are smaller (approximately 10^{-3} to 10^{-4} MPa) than the triggering threshold (0.01 MPa),
265 implying the stress interaction between those two events are weak. At the hypocenter of the
266 14YT, the static and viscoelastic dCFSs induced by 08YT are comparable with the triggering
267 threshold, which implies a weak interaction. The static and viscoelastic dCFSs induced by
268 12YT on 14YT are insignificant (approximately 10^{-4} MPa), implying the stress interaction
269 between them are very weak. As for the 20YT, the dCFS induced by the 08YT is small
270 (approximately 10^{-3} MPa), the dCFS induced by the 12YT is larger (approximately 10^{-2} MPa)
271 than triggering threshold and the dCFS induced by the 14YT is remarkable (approximately
272 10^{-1} MPa). This finding implies that the proceeding Yutian earthquakes contribute the
273 occurrence of 20YT. The largest triggering contribution comes from the 14YT (approximately
274 71%≈0.10523/0.1477).

275

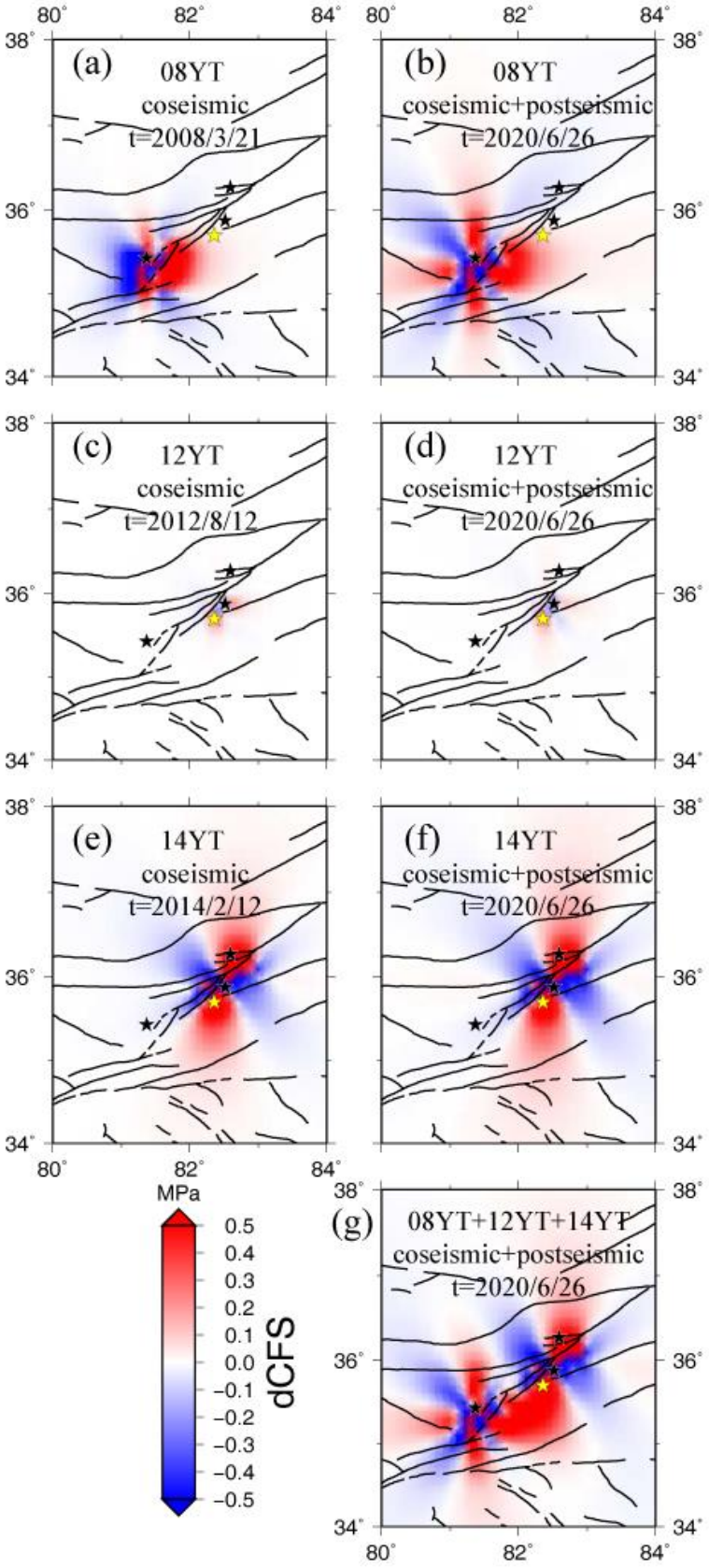

276

277 Figure 4 Spatial distribution of dCFS at hypocenter of 20YT induced by proceeding Yutian

earthquakes. (a), (c) and (e) show static (coseismic) dCFS induced by the 08YT, 12YT and 14YT. (b), (d) and (f) show viscoelastic (coseismic and postseismic) dCFS induced by the 08YT, 12YT and 14YT. (g) Combined dCFS induced by all three Yutian earthquakes (08YT, 12YT and 14YT). The black lines represent major faults, black stars indicate 08YT, 12YT and 14YT, and yellow star shows location of 20YT. The resolving depth is 15 km and strike, dip, rake angles are 213°, 52°, -66° (GCMT), respectively.

The triggering contribution from 08YT, 12YT and 14YT to 20YT can also be clearly identified from spatial distribution of dCFS (Figure 4). From Figure 4(a)-(g), the epicenter of the 20YT always fall into positive zone of dCFS. The uncertainties of dCFS impacted by resolving depth and friction coefficient are also investigated in the Supplementary Information, and the results are similar. The 08YT and 14YT generate a wider spatial stress disturbance than 12YT due to their larger magnitudes. It is also interesting that several faults between epicenters of 08YT and 20YT experience a positive dCFS induced by 08YT and a negative dCFS induced by 14YT at the same time. The seismic hazard in this region may be paid more attention.

4. Discussion

4.1 Uncertainties of calculations of dCFSs

Large uncertainties of calculations of dCFSs caused by non-unique solutions of source slip distribution and poor-constrained parameters (e.g., friction coefficient, resolving depth) may weaken results based on dCFS (*Jia et al.*, 2018; *Steacy et al.*, 2004; *Wang et al.*, 2014a). *Jia et al.* (2018) have shown that large uncertainties of dCFS may lead different even conflicting results in the case of 2008 Wenchuan and 2017 Jiuzhaigou earthquakes. One way to minimize uncertainties is properly choosing source models and parameters. On the other hand, ranges of uncertainties are also investigated by calculating dCFSs using different possible parameters. As described in calculation of dCFS, the finite fault models of 08YT (*Elliott et al.*, 2010) and 14YT (*Zhang et al.*, 2014) are chosen because they are best choices for representative models of source slip distributions. As for 12YT, there is no other way to use a better source model

than the synthetic slip model estimated from the empirical relations of *Wells and Coppersmith* (1994). The uncertainties due to different choices of friction coefficient and resolving depth are investigated. A higher (0.8) or lower (0.2) value of friction coefficient does not remarkably influence results of dCFS for this case (Tabls S1 and S2, Figure S4 and S5). Calculations of using different resolving depths (10 km and 15 km) show that the resolving depth also does not change results of dCFS much (Figure S6). Thus, our conclusions based on dCFS are still valid considering uncertainties.

4.2 Validation of Coulomb failure hypothesis

Stress interactions among multiple faults in a local scale region provide good opportunity to test Coulomb failure hypothesis. Previous case studies have shown some successful examples from view of stress transfer (*Freed and Lin*, 2001; *Jia et al.*, 2014; *Jia et al.*, 2018; *Pope and Mooney*, 2020; *Quigley et al.*, 2016). However, as mentioned above, calculations of dCFS suffer large uncertainties and results are subjective in some degree (e.g., choices of source models and parameters are subjective). It is necessary to verify results of dCFS from another perspective. The statistical insight (e.g., ETAS model) provides a good cross reference for its objectivity and small uncertainties. Background probabilities estimated from formula (1) provide information of whether earthquakes are triggered or tectonic events. A low value (close to zero) of background probability indicates a triggered event, which usually experiences a positive dCFS induced by other major earthquakes. A high value (close to 1.0) of background probability represents an independent event, which usually have no stress interaction with other earthquakes and results from tectonic loading. *Jia et al.* (2018) have conducted a statistical analysis in the Jiuzhaigou region to clarify the triggering relationship of the 2008 Wenchuan and 2017 Jiuzhaigou earthquakes, which cannot be well deduced from the results of dCFS. In this study, the background probability 12YT (0.97) coincides with positive dCFSs calculated on its hypocenter induced by other major earthquakes (-1.5004×10^{-4} MPa). And, background probabilities of the 14YT (1.5×10^{-3}) and 20YT (8.7×10^{-5}) coincide with positive dCFSs calculated on their hypocenters induced by proceeding Yutian earthquakes (0.003582 MPa for 14YT and 0.1477 MPa for 20YT). From those two different

kinds of perspective, the stress interaction among multiple faults or earthquakes can be comprehensively investigated.

5. Conclusion

The June 26, 2020 Mw 6.3 Yutian earthquake, occurred in western boundary of Bayan Har block, is the fourth M6+ earthquake in this region since occurrence of 08YT. We have investigated the stress interaction among the 08YT, 12YT, 14YT and 20YT by applying the ETAS model and calculating dCFS. The background probabilities of 08YT, 12YT, 14YT and 20YT are 0.87, 0.97, 1.5×10^{-3} and 8.7×10^{-5}, respectively, implying that the 08YT and 12YT are more like background earthquakes and 14YT and 20YT are triggered events. The epicenters of 08YT, 12YT, 14YT and 20YT are located at highest background seismicity (approximately 0.1 M≥3.5 events/degree^2/yr), where is a complex stepover zone with multiple normal faults. The viscoelastic dCFS induced by proceeding Yutian earthquakes on hypocenters of 12YT, 14YT and 20YT are -1.5004×10^{-4}, 3.5820×10^{-3} and 1.4770×10^{-1} MPa, respectively. Those two kinds of evidence are consistent with each other, implying a local stress interaction among those four Yutian earthquakes. For the Bayan Har block, both the tectonic loading and local stress interaction along its boundary could lead to seismic activities. As a result, the current tectonic movement of the Bayan Har block is relatively active, and the seismic hazard along its boundaries should be paid more attention.

Acknowledgement

The catalog used in this study is from China Earthquake Data Center (CEDC, http://data.earthquake.cn/index.html). The PSGRN/PSCMP code is provided by Prof. Rongjiang Wang. We benefit from discussion with Fuqiang Shi and Hurong Duan. This research is jointly supported by the National Key R&D Program of China (2018YFC1503400), the National Natural Science Foundation of China projects (41804048, U2039204), China Seismic Experimental Site (2019CSES0106), China Postdoctoral Science Foundation (2020M673469), and the Fundamental Research Funds for the Central Universities (3102019ZDHKY12). Generic Mapping Tool mapping software (*Wessel and*

365 *Smith*, 1991) is used to prepare some figures.

366

367 **References**

368 Bie, L., and I. Ryder (2014), Recent seismic and aseismic activity in the Ashikule stepover zone, NW
369 Tibet, *Geophysical Journal International*, *198*(3), 1632-1643.
370 Elliott, J. R., R. J. Walters, P. C. England, J. A. Jackson, Z. Li, and B. Parsons (2010), Extension on the
371 Tibetan plateau: recent normal faulting measured by InSAR and body wave seismology, *Geophysical*
372 *Journal International*, *183*(2), 503–535.
373 Freed, A. M., and J. Lin (2001), Delayed triggering of the 1999 Hector Mine earthquake by viscoelastic
374 stress transfer, *Nature*, *411*(6834), 180-183, doi:10.1038/35075548.
375 Harris, R. A. (1998), Introduction to Special Section: Stress Triggers, Stress Shadows, and Implications
376 for Seismic Hazard, *Journal of Geophysical Research*, *103*(10), 24347-24358.
377 Harte, D. (2015), Model parameter estimation bias induced by earthquake magnitude cut-off,
378 *Geophysical Journal International*, *204*(2), 1266-1287, doi:doi:10.1093/gji/ggv524.
379 Jia, K., S. Zhou, and R. Wang (2012), Stress Interactions within the Strong Earthquake Sequence from
380 2001 to 2010 in the Bayankala Block of Eastern Tibet, *Bulletin of the Seismological Society of America*,
381 *102*(5), 2157-2164.
382 Jia, K., S. Zhou, J. Zhuang, and C. Jiang (2014), Possibility of the Independence between the 2013
383 Lushan Earthquake and the 2008 Wenchuan Earthquake on Longmen Shan Fault, Sichuan, China,
384 *Seismological Research Letters*, *85*(1), 60-67, doi:10.1785/0220130115.
385 Jia, K., S. Zhou, J. Zhuang, C. Jiang, Y. Guo, Z. Gao, and S. Gao (2018), Did the 2008 Mw 7.9
386 Wenchuan earthquake trigger the occurrence of the 2017 Mw 6.5 Jiuzhaigou earthquake in Sichuan,
387 China?, *Journal of Geophysical Research: Solid Earth*, *123*(4), 2965-2983.
388 Jiang, C., L. Han, and L. Guo (2014), Parameter Characteristics in the Early Period of Three
389 Earthquake Sequences in the Yutian, Xiniiang Since 2008, *Acta Seis-mologiea Sinica*, *36*(2), 165-174.
390 Kroll, K. A., K. B. Richards‐Dinger, J. H. Dieterich, and E. S. Cochran (2017), Delayed seismicity
391 rate changes controlled by static stress transfer, *Journal of Geophysical Research: Solid Earth*, *122*(10),
392 7951-7965.
393 Li, Y., L. Chen, S. Liu, S. Yang, X. Yang, and G. Zhang (2015), Coseismic Coulomb stress changes
394 caused by the Mw6.9 Yutian earthquake in 2014 and its correlation to the 2008 Mw7.2 Yutian
395 earthquake, *Journal of Asian Earth Sciences*, *105*, 468-475.
396 Ogata, Y. (1998), Space-Time Point-Process Models for Earthquake Occurrences, *Annals of the*
397 *Institute of Statistical Mathematics*, *50*(2), 379-402, doi:10.1023/A:1003403601725.
398 Ogata, Y. (2004), Space-time model for regional seismicity and detection of crustal stress changes,
399 *Journal of Geophysical Research*, *109*(B3), 235-273.
400 Ogata, Y., and J. Zhuang (2006), Space–time ETAS models and an improved extension, *Tectonophysics*,
401 *413*(1–2), 13-23, doi:10.1016/j.tecto.2005.10.016.
402 Pollitz, F. F., and C. Cattania (2017), Connecting crustal seismicity and earthquake‐driven stress
403 evolution in Southern California, *Journal of Geophysical Research: Solid Earth*, *122*(8), 6473-6490.
404 Pope, N., and W. D. Mooney (2020), Coulomb stress models for the 2019 Ridgecrest, California
405 earthquake sequence, *Tectonophysics*, *791*, 228555.
406 Quigley, M. C., M. W. Hughes, B. A. Bradley, S. van Ballegooy, C. Reid, J. Morgenroth, T. Horton, B.

Duffy, and J. R. Pettinga (2016), The 2010–2011 Canterbury earthquake sequence: Environmental effects, seismic triggering thresholds and geologic legacy, *Tectonophysics*, *672*, 228-274.

Ramos, M. D., J. C. Neo, P. Thakur, Y. Huang, and S. Wei (2020), Stress Changes on the Garlock fault during and after the 2019 Ridgecrest Earthquake Sequence, *Bulletin of the Seismological Society of America*.

Sornette, D., and M. J. Werner (2005), Constraints on the size of the smallest triggering earthquake from the epidemic ‐ type aftershock sequence model, Båth's law, and observed aftershock sequences, *Journal of Geophysical Research*, *110*(B8), B08304, doi:10.1029/2004JB003535.

Steacy, S., J. Gomberg, and M. Cocco (2005), Introduction to special section: Stress transfer, earthquake triggering, and time-dependent seismic hazard, *Journal of Geophysical Research*, *110*(B5), doi:10.1029/2005JB003692.

Steacy, S., D. Marsan, S. S. Nalbant, and J. McCloskey (2004), Sensitivity of static stress calculations to the earthquake slip distribution, *Journal of Geophysical Research: Solid Earth (1978–2012)*, *109*(B4).

Stein, R. S. (1999), The role of stress transfer in earthquake occurrence, *Nature*, *402*(6762), 605-609, doi:10.1038/45144.

Tapponnier, P., X. Zhiqin, F. Roger, B. Meyer, N. Arnaud, G. Wittlinger, and Y. Jingsui (2001), Oblique stepwise rise and growth of the Tibet Plateau, *science*, *294*(5547), 1671-1677.

Taylor, M., and A. Yin (2009), Active structures of the Himalayan-Tibetan orogen and their relationships to earthquake distribution, contemporary strain field, and Cenozoic volcanismActive structures on the Tibetan plateau and surrounding regions, *Geosphere*, *5*(3), 199-214.

Toda, S., R. S. Stein, G. C. Beroza, and D. Marsan (2012), Aftershocks halted by static stress shadows, *Nature Geoscience*, *5*(6), 410-413.

Toda, S., R. S. Stein, K. Richards-Dinger, and S. B. Bozkurt (2005), Forecasting the evolution of seismicity in southern California: Animations built on earthquake stress transfer, *Journal of Geophysical Research*, *110*(B5), doi:10.1029/2004JB003415.

Utsu, T., Y. Ogata, S. Ritsuko, and Matsu'ura (1995), The Centenary of the Omori Formula for a Decay Law of Aftershock Activity, *Journal of Physics of the Earth*, *43*(1), 1-33.

Wan, Y., and Z.-K. Shen (2010), Static Coulomb stress changes on faults caused by the 2008 Mw 7.9 Wenchuan, China earthquake, *Tectonophysics*, *491*(1–4), 105-118, doi:10.1016/j.tecto.2010.03.017.

Wang, J., C. Xu, J. T. Freymueller, and Z. Li (2017), Probing Coulomb stress triggering effects for a Mw > 6.0 earthquake sequence from 1997 to 2014 along the periphery of the Bayan Har block on the Tibetan Plateau, *Tectonophysics*, *694*, 249-267, doi:https://doi.org/10.1016/j.tecto.2016.11.009.

Wang, J., C. Xu, J. T. Freymueller, Z. Li, and W. Shen (2014a), Sensitivity of Coulomb stress change to the parameters of the Coulomb failure model: A case study using the 2008 M w 7.9 Wenchuan earthquake, *Journal of Geophysical Research*, *119*(4), 3371–3392.

Wang, Y., F. Wang, M. Wang, Z. K. Shen, and Y. Wan (2014b), Coulomb Stress Change and Evolution Induced by the 2008 Wenchuan Earthquake and its Delayed Triggering of the 2013 Mw 6.6 Lushan Earthquake, *Seismological Research Letters*, *85*(1), 52-59.

Wells, D. L., and K. J. Coppersmith (1994), New empirical relationships among magnitude, rupture length, rupture width, rupture area, and surface displacement, *Bulletin of the seismological Society of America*, *84*(4), 974-1002.

Wessel, P., and W. H. F. Smith (1991), Free software helps map and display data, *Eos Trans. AGU*, *72*(41), 441-446, doi:10.1029/90eo00319.

Wiemer, S. (2001), A software package to analyze seismicity: ZMAP, *Seismological Research Letters*, *72*(3), 373-382.

Wiemer, S., and M. Wyss (2000), Minimum Magnitude of Completeness in Earthquake Catalogs: Examples from Alaska, the Western United States, and Japan, *Bulletin of the Seismological Society of America*, *90*(4), 859-869.

Xiong, X., B. Shan, Y. Zheng, and R. Wang (2010), Stress transfer and its implication for earthquake hazard on the Kunlun Fault, Tibet, *Tectonophysics*, *482*(1–4), 216-225, doi:10.1016/j.tecto.2009.07.020.

Xu, X., X. Tan, G. Yu, G. Wu, W. Fang, J. Chen, H. Song, and J. Shen (2013), Normal-and oblique-slip of the 2008 Yutian earthquake: evidence for eastward block motion, northern Tibetan Plateau, *Tectonophysics*, *584*, 152-165.

Zhang, P., Q. Deng, G. Zhang, J. Ma, W. Gan, W. Min, F. Mao, and Q. Wang (2003), Active tectonic blocks and strong earthquakes in the continent of China, *Science in China Series D: Earth Sciences (in Chinese)*, *46*(2), 13-24.

Zhang, Y., L.-s. Xu, Y.-T. Chen, and R.-j. Wang (2014), Fast inversion for the rupture process of the 12 February 2014 Yutian MW6. 9 earthquake: Discussion on the impacts of focal mechanisms on rupture process inversions, *Acta Seismologica Sinica*, *36*(2), 159-164.

Zhao, L., L. Zhao, and X. Xie (2016), Static Coulomb stress changes and seismicity rate in the source region of the 12 February, 2014 M W 7.0 Yutian earthquake in Xinjiang, China, *Chinese Journal of Geophysics*, 3732-3743.

Zhuang, J., C.-P. Chang, Y. Ogata, and Y.-I. Chen (2005), A study on the background and clustering seismicity in the Taiwan region by using point process models, *J. Geophys. Res.*, *110*(B5), doi:10.1029/2004jb003157.

Zhuang, J., Y. Ogata, and D. Vere-Jones (2004), Analyzing earthquake clustering features by using stochastic reconstruction, *Journal of Geophysical Research: Solid Earth*, *109*(B5), B05301, doi:10.1029/2003JB002879.